ADVANCED MATERIALS TECHNOLOGIES
www.advmattechnol.de

# Integrated Optoelectronic Devices Using Lab-On-Fiber Technology

*Armando Ricciardi, Michael Zimmer, Norbert Witz, Alberto Micco, Federica Piccirillo, Martino Giaquinto, Mathias Kaschel, Joachim Burghartz, Michael Jetter, Peter Michler, Andrea Cusano,* and Simone Luca Portalupi**

**Silica fibers are nowadays cornerstones in several technological implementations from long-distance communication, to sensing applications in many scenarios. To further enlarge the functionalities, the compactness, and the performances of fiber-based devices, one needs to reliably integrate small-footprint components such as sensors, light sources, and detectors onto single optical fiber substrates. Here, a novel proof of concept is presented to deterministically integrate optoelectronic chips onto the facet of an optical fiber, further implementing the electrical contacting between the chip and fiber itself. The CMOS-compatible procedure is based on a suitable combination of metal deposition, laser machining, and micromanipulation, directly applied onto the fiber tip. The proposed method is validated by transferring, aligning, and bonding a quantum-well based laser on the core of a multimode optical fiber. The successful monolithic device integration on fiber shows simultaneously electrical contacting between the laser and the ferrule, and 20% light in-coupling in the fiber. These results pave new ways to develop the next generation of optoelectronic systems on fiber. The technological approach will set a new relevant milestone along the lab-on-fiber roadmap, opening new avenues for a novel class of integrated optoelectronic fiber platforms, featuring unrivaled miniaturization, compactness, and performances levels, designed for specific applications.**

## 1. Introduction

Optical fibers are a cornerstone technology in many different aspects of fundamental science and real-world applications. Nowadays, this technology is ubiquitous in telecom systems for long-distance implementation, and also boosts a high level of maturity in other sectors beyond information and communication technologies (ICT), such as medicine, endoscopy, and imaging devices. The past two decades, in fact, marked a turning point in the optical fiber technology roadmap. The "optical fiber revolution" started at the beginning of the century, with the development of photonic crystal fibers,[1,2] continued with the creation of multimaterial fibers,[3] and it is still underway. In this respect, the constant progress in materials science and nanotechnologies pushed optical fibers to a new level.[4] In the spirit of the Lab-on-Fiber vision, most of micro- and nanofabrication techniques were judiciously customized to work with optical fibers, and nowadays it is possible to conceive complex 3D objects fully integrated onto the fiber facet.[5,6] The integration of different kinds of materials and structures onto optical fibers led to the development of advanced multifunctional optrodes exploitable in many contexts of sensing applications.[7]

Recent and relevant examples of the current state of the optical fiber technological revolution are the demonstrations of all-in-fiber nano-endoscopes for Optical Coherence Tomography,[8] high-sensitivity transducers for photo-acoustic and ultrasound imaging,[9] nano-probes integrating smart materials for label-free small molecule detection and nano-opto-mechanical-actuation,[10,11] surface enhanced Raman scattering imaging,[12] and meta-surfaces designed for optical processing and computing.[13,14]

Despite the high degree of integration at sub-wavelength scale of components on the same platform, the optical fiber probes are still used in combination with external bulk sources, detectors, and "off-fiber" electrically driven components. This clearly impacts the overall device footprint and achievable scalability. Moreover, the fiber-to-chip coupling in hybrid photonic integrated circuits still represents a major challenge, which limits their efficacy in real application scenarios. For this reason, recent efforts of the scientific community are also being

A. Ricciardi, A. Micco, F. Piccirillo, M. Giaquinto, A. Cusano
Optoelectronics Group
Department of Engineering
University of Sannio
Benevento 82100, Italy
E-mail: a.cusano@unisannio.it

M. Zimmer, N. Witz, M. Jetter, P. Michler, S. L. Portalupi
Institut für Halbleiteroptik und Funktionelle Grenzflächen
Center for Integrated Quantum Science and Technology (IQST)
and SCoPE
University of Stuttgart
Allmandring 3, Stuttgart 70569, Germany
E-mail: s.portalupi@ihfg.uni-stuttgart.de

M. Kaschel, J. Burghartz
Institut für Mikroelektronik Stuttgart (IMS CHIPS)
Stuttgart 70569, Germany

The ORCID identification number(s) for the author(s) of this article can be found under https://doi.org/10.1002/admt.202101681.



**DOI: 10.1002/admt.202101681**

devoted to find new solutions for highly efficient and position-tolerant coupling.[15,16]

Considering the technological maturity achieved so far, at both fabrication and application level, it is now expected a further step-ahead along the lab-on-fiber technological roadmap.[4] The new frontier should be the creation of all-in-fiber optoelectronic autonomous systems, able to achieve a full control over the flow of light, from its generation up to its detection, passing through its manipulation. In fact, the combination of all the functional components of a generic optical system commonly employed in communication and sensing fields (light source, optical waveguide, photodetector, etc.) into a single compact unit, will change completely the existent paradigm of discrete systems assembled for specific applications, opening a new technological roadmap toward next generation of optoelectronic devices on fiber. The idea was proposed by He et al. who integrated precisely doped semiconductor materials and high-quality rectifying semiconductor junctions into microstructured optical fibers, enabling high-speed, in-fiber functionalities such as photodetection at telecommunications wavelengths.[17] Recently, M. Rein et al. developed an interesting technique to incorporate functional semiconductor devices and electrical conductors into a polymer-clad preform.[18] This approach was applied to produce a linear array of semiconductor devices uniformly spaced along the fiber length (fiber size as small as 350 μm × 350 μm) and electrically connected in parallel. This new generation of fibers can be applied in different domains and in particular in wearable technologies for health monitoring. Y. Xiong et al. successfully demonstrated the integration of photodetectors based on both a (micrometer-scale) multilayer graphene-$MoS_2$-$WS_2$ heterostructure film,[19] and a ≈63 nm thick $COF_{ETBC\text{-}TAPT}$-graphene heterostructure film[20] on the optical fiber tip.

In this framework, here we propose and demonstrate a proof of concept to integrate, directly onto the tip of an optical fiber facet, a compact optoelectronic chip, in a deterministic fashion. The fabrication approach has been developed in order to be fully compatible with the CMOS technology and with mass production systems employing industrial, automatized machines. The use of a deterministic approach represents a fundamental step forward to realize high-efficiency optical packaging and integration with a very high fabrication yield.

In our technique, laser micro-machining is used to precisely realize an aperture on the metalized fiber facet, in correspondence with its core, as well as a set of alignment markers utilized in the successive fabrication steps. Then, the optoelectronic component is transferred, aligned (with the aid of a micromanipulator, compatible with high throughput production systems exploitable in future implementations), and bonded onto the fiber tip. The markers enable the deterministic alignment of the light-emitting element on top of the fiber core with sub-micrometric precision. The entire process enables the implementation of the electrical contacts directly on the fiber tip, drastically reducing the overall device footprint. The use of a deterministic approach, in our opinion, represents the first milestone to pave new avenues for the development of the next generation of all-fiber optoelectronic devices with unrivaled coupling efficiency and fabrication yield.

As a proof of principle demonstration, our approach here is applied to integrate a compact electrically driven quantum-well vertical-cavity surface-emitting laser (QW-VCSEL) onto the facet of a multimode fiber. The employed laser structure has been grown using metal–organic vapor-phase epitaxy (MOVPE), being the most utilized technique for the industrial realization of efficient light sources. VCSELs, in particular, are highly appealing as laser sources for a variety of applications, being compact and flexible in operation wavelength design.[21–23]

The emission wavelength of the used VCSEL device lies in the red spectral range ≈670 nm, commonly used for polymer-optical-fiber (POF) data transmission.[24]

It is important to stress that the choice of integrating the above-mentioned VCSEL device does not make our procedure to lose generality since it is applicable to any optoelectronic components chosen to meet the requirements of the specific application (LED, detectors...). Moreover, the proposed technique can be thus applied in hybrid photonic systems to the multiplicity of optical fibers, thus substituting the bulky on-chip mode converters. In particular, our approach can be used to integrate onto the fiber facet even quantum devices emitting single, indistinguishable, and entangled photons. A fiber-coupled source of nonclassical light is highly attractive for a large variety of quantum optical experiments, where a mechanically stable, fiber-coupled source would allow for long integration time without requiring constant realignment.[25–29] This would open the route for a novel class of integrated Lab-on-Fiber optoelectronic.

## 2. Results

### 2.1. Fabrication and Characterization of the QW-VCSEL

The electrically driven QW-VCSEL used in our experiments is schematically shown in **Figure 1**a. An active layer based on GaInP QWs in $Al_{0.33}GaInP/Al_{0.55}GaInP$ barriers is grown between two doped distributed Bragg reflectors (bottom n-doped and top p-doped, respectively). Mesa structures are fabricated and lateral oxidation is employed to realize an aperture for the flowing current. Details on the fabrication procedure are given in the Experimental Section. In order to achieve the smallest possible footprint for the final device, the VCSEL sample was cleaved into pieces of roughly 500 μm × 500 μm (see Figure 1b), therefore much smaller than the fiber ferrule (compare the microscope picture of an example piece in Figure 1b with the fiber ferrule in **Figure 2**). Specifically, the sample is cleaved to keep four mesa structures on the chip. After cleaving, all realized devices were thoroughly measured in order to have a precise estimation of the performances of the chosen laser before the integration (details on the experimental setup are provided in the Supporting Information). Each of the four lasers was individually contacted (and the measurements repeated for multiple chips) with electrical probes while the chip is being installed on a thermal heat sink. In this way, emission power measurements over current were conducted for different values of the heat sink temperature (see Figure 1c). For all devices, a similar output power at thermal rollover was measured for the same measurement

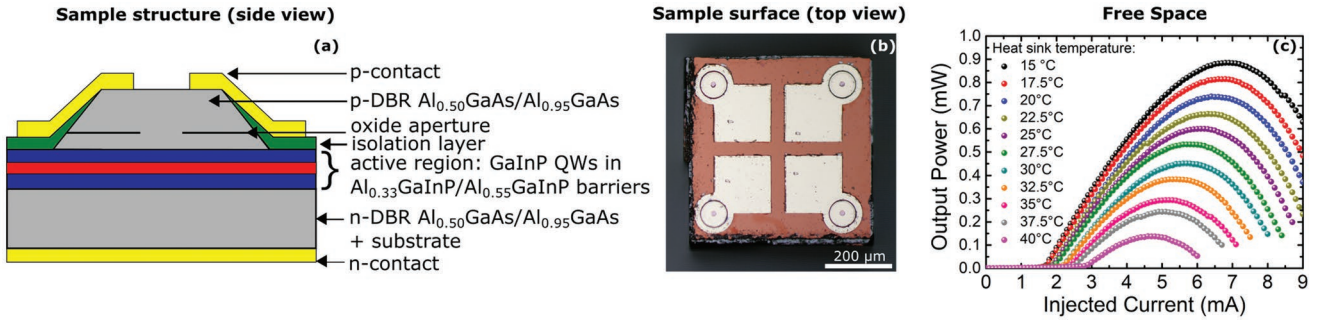


**Figure 1.** a) Schematic (cross section view) of the VCSEL structure. b) Microscope picture of the top device surface. c) Laser output power measured as a function of the injected current for different heat sink temperature.

conditions (see Figure 1c and Supporting Information). A colder heatsink results in a lower local laser temperature, hence in a thermal rollover at higher currents. Being a characteristic of the VCSEL device, special attention is emphasized here toward the device behavior around the thermal rollover. In order to be able to identify the working point of the QW-VCSEL, when integrated on the fiber facet, the emission spectra were also acquired for different heat sink temperatures and injection currents above the lasing threshold. Additionally, the laser beam profile was recorded for a later comparison with the integrated device.

Once verified that all lasers have a similar performance, we selected one for further integration on the fiber tip (see Sections 2.2 and 2.3). The investigated final device makes use of one laser to be coupled into the fiber core, while the other three are kept in place to ensure the planarity of the chip after integration on the fiber: indeed, as it can be seen from Figure 1a, the laser structure has a height of 3.8 µm over the chip surface and bonding pads. These large bonding pads are used to ensure the electrical contact of the chosen device with the metalized fiber ferrule (see Section 2.2).

### 2.2. Markers and Aperture Realization on the Optical Fiber Tip

The fiber used in our experiments is a ceramic ferrule-top step index multimode fiber (0.5-meter-long), with core/cladding diameters of 105/125 µm and a numerical aperture NA = 0.22 (model: QMMJ-2.5S2.5S-IRVIS-105/125-1-0.5 from OZ Optics). No pretreatment or polishing of the fiber tip was made at this stage. A 150 nm thick gold (Au) film was deposited by means of electron beam evaporation (Kenosistec CL400C) on the polished end. A thin (≈10 nm) titanium (Ti) film was used as an adhesion layer. The ferrule top was mounted on a customized holder with an angle of 60° with respect to the evaporation direction in order to create a gold layer on both the top and side of the fiber. The deposition rates were 0.1 and 0.5 nm $s^{-1}$ for the Ti and Au films, respectively.

The gold layer was successively patterned via a UV micromachining laser process to realize both the circular hole in correspondence to the fiber core and the aligning markers. All the markers have a width of 15 µm (see Figure 2a) and they were realized in accordance with the actual sample geometry derived from the microscope images of the chip (Figure 1b).

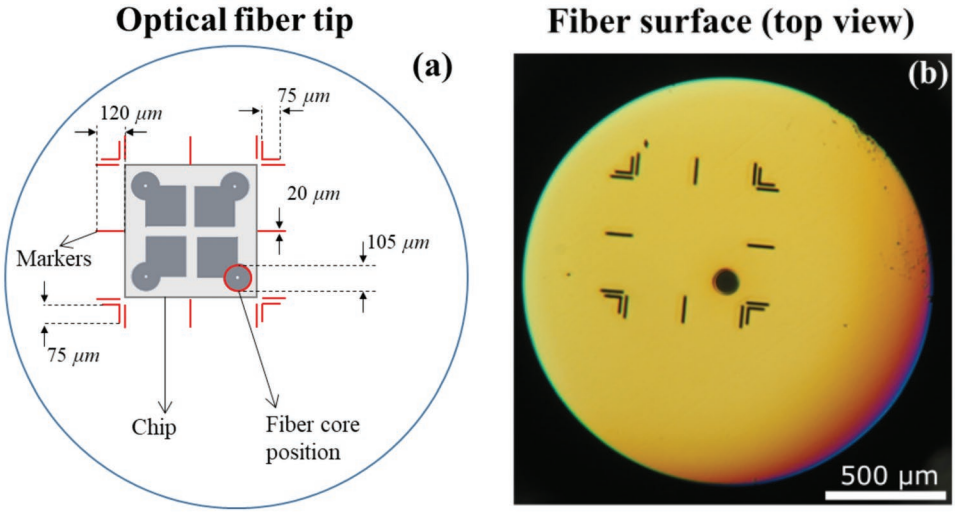


**Figure 2.** a) Schematics of the markers dimensions based on the actual chip size. b) Top view of the metalized and laser-machined fiber ferrule. An opening aligned to the fiber core, as well as alignment markers are clearly visible. The markers were realized asymmetrically over the fiber core to ensure the alignment of the chosen VCSEL to the aperture.

This ensures that the emitting device is precisely aligned to the fiber core, simultaneously providing electrical contact between the chip and the fiber ferrule.

The equipment used (OPTEC LB 1000) consists of an excimer laser (KrF, $\lambda$ = 248 nm) with pulse width of ≈5–6 ns. A plastic holder has been used to keep the ferrule top perpendicular to the focused laser beam during the ablation process and fixed to the stage. The laser energy was 9 mJ, the repetition rate 60 Hz. The motion speed of the stage was 0.5 mm $s^{-1}$. Figure 2b shows the top view of the fiber tip after the micromachining process.

### 2.3. Integration of the QW-VCSEL onto the Fiber Tip and Electrical Contacting

The integration procedure is schematically shown in **Figure 3**. First, two types of glue were carefully deposited on the patterned fiber tip: the central spot (corresponding to the fiber core) was covered with index-matching glue, to minimize optical losses due to refractive index mismatch (see Figure 3a,d and Supporting Information). Moreover, to ensure the electrical contact between the p-contact of the VCSEL and the gold coating of the optical fiber, an electrically conductive glue (silver epoxy) was applied to the fiber ferrule (outside the fiber core) in correspondence with the position of the contacts: being the contact pads close to each other and the conductive epoxy placed by hand, all four lasers resulted to be connected (see Supporting Information). In this realization, robust adhesion and mechanical stability are ensured by the presence of conducting epoxy and further by the cured refractive index matching glue. Thanks to the deterministic alignment, only the selected VCSEL is overlapping the fiber core and, hence, the emitted light is coupled, while the other lasers are simply reflected by the deposited metallic surface. At this point, the performances of the laser are preserved and only a higher current is necessary to reach the thermal rollover. Interestingly, thanks to the sample geometry, the three non-used lasers serve to ensure the planarity of the sample when placed on the fiber. Indeed, being all lasers at the same height, while the rest of the surface is etched down, they all four act as legs when brought in contact with the fiber ferrule surface. The aim of our work, at this stage, was to demonstrate the validity of the proposed fabrication approach by coupling light emitted from one single laser to the optical fiber. However, in future realizations, the laser array can be mounted on multicore fibers in such a way that different lasers are coupled in different cores achieving interesting multiplexing and/or multisensing capabilities. Furthermore, employing precise epoxy delivery tools will give us the possibility to enhance the alignment precision and decrease the amount of glue required

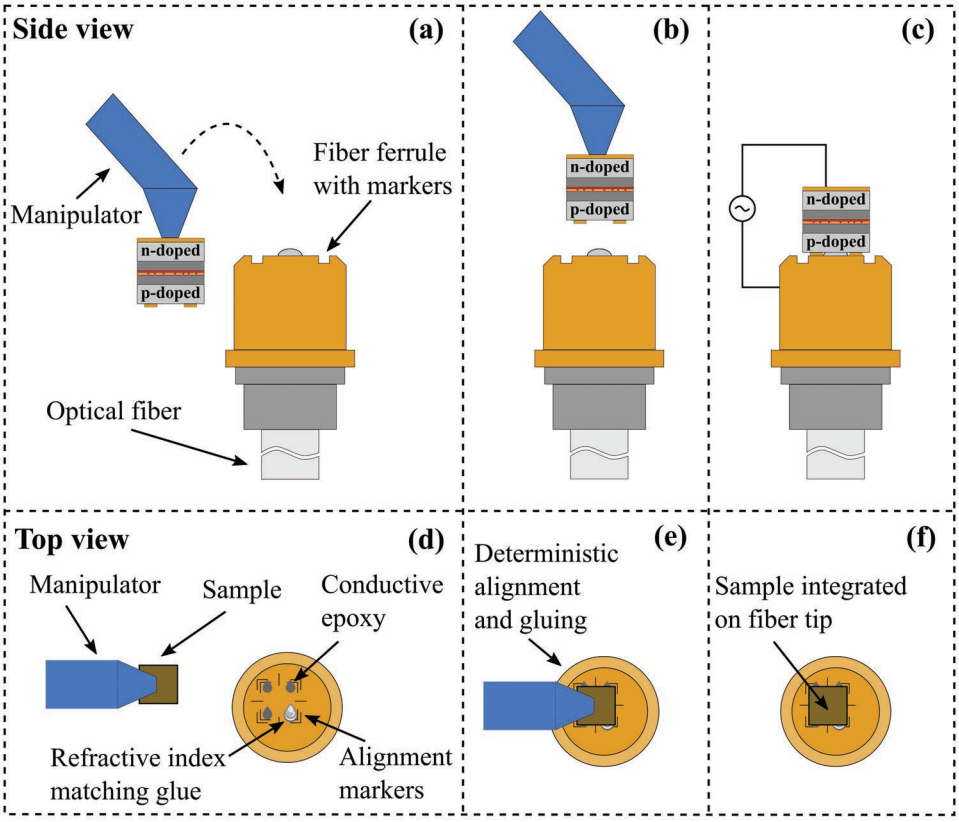


**Figure 3.** Scheme of integration and alignment procedure from a–c) side and d–f) top view. The fiber ferrule with markers is prepared by adding refractive index matching glue and conductive epoxy while a micromanipulator is employed to pick and move the sample (a,d). The selected active area of the sample is deterministically aligned on the fiber core using the fabricated markers (b,e) and pressed on the fiber tip. The final device (c,f) is ready to be contacted and powered. While the top sample metal contacts are now electrically contacted with the ferrule, the sample bottom contact is separately accessible. 3D sketches and microscope pictures of the fiber ferrule along the process are shown in the Supporting Information.

for bonding. The index matching glue and the conductive adhesive have been deposited in such a way to stay separated also after the sample integration, since an intermixing would cause metal particles to diffuse into the transparent glue, introducing scattering losses that reduce the coupling efficiency.

Finally, the laser sample was placed on the fiber tip and positioned considering the calculated coordinates relative to the markers (see Figure 3b,e for the alignment procedure and Figure 3c,f for the integration). Specifically, the QW-VCSEL was previously characterized via optical microscopy to precisely measure the position of the lasers with respect to the sample edges (see Figure 1b). This characterization allows for the successive deterministic alignment of the flipped sample with respect to the markers defined on the fiber tip, thus maximizing the overlap between the optically active area and the core, preventing the covering of the opened window by the metal contacts.

In this first experiment, the transferring step was made manually by means of a vacuum pick-up tool and an optical microscope. However, for future realizations, it is possible to use motorized micromanipulators that allow to achieve together sub-micrometric precision and high fabrication yield. The approach described here is thus well-suited for large-scale industrial processing since image recognition algorithms will allow for an automatic alignment of the sample with respect to the fabricated markers. After the gluing, the top contact of the sample results to be electrically connected with the gold-coated fiber ferrule and the sample bottom contact can be treated independently (see Figure 3c).

Finally, the sample was put in contact with a custom-made electrical plug that was realized via Cu-coated PCB, with a metallic pin connecting the sample back contact (see Supporting Information for a complete description). The top sample contacts, glued to the fiber ferrule, were then connected via the side of the fiber ferrule. We would like to point out that the bulk PCB was used at this stage just to assess the technological approach and evaluate the coupling efficiency performance. In any case, since the optical fiber is coated with gold around the core and along the cladding of the fiber itself, our configuration makes it possible to directly support the miniaturized electronic chip so that the overall size of the integrated device remains compact.

### 2.4. Fiber-Integrated Sample Characterization

Once the preselected VCSEL has been integrated on the fiber, measurements were conducted to quantify the laser behavior and comparing it with the free space scenario. The most interesting parameter is the coupling efficiency, i.e., the percentage of light that is actually coupled in the core. For the fiber integrated device, we found that the maximum power is 0.24 mW (**Figure 4**a). This measurement has been conducted by directly plugging the output of the fiber to the same power meter employed in the free space measurements. To accurately quantify how this value relates to the free space one, it is imperative to compare the laser under the same operation conditions in both scenarios (i.e., free space and fiber integrated). Indeed, it is known that the actual local VCSEL temperature influences the maximally achievable output power at thermal rollover, as it can be inferred from Figure 1c. On the other hand, a direct evaluation of the VCSEL temperature itself can be quite challenging: when placed on the heat sink, the set temperature only refers to the sample holder and it is not the same of (despite it is proportional to) the actual laser temperature. Additionally, after integration on the fiber, no thermal sink was employed and only heat transfer to the surrounding was allowed. For this reason, the determination of the operation conditions was done further measuring the emission spectrum at thermal rollover. Indeed, observing the same emission wavelength at thermal rollover implies comparable working conditions, i.e., a comparable local

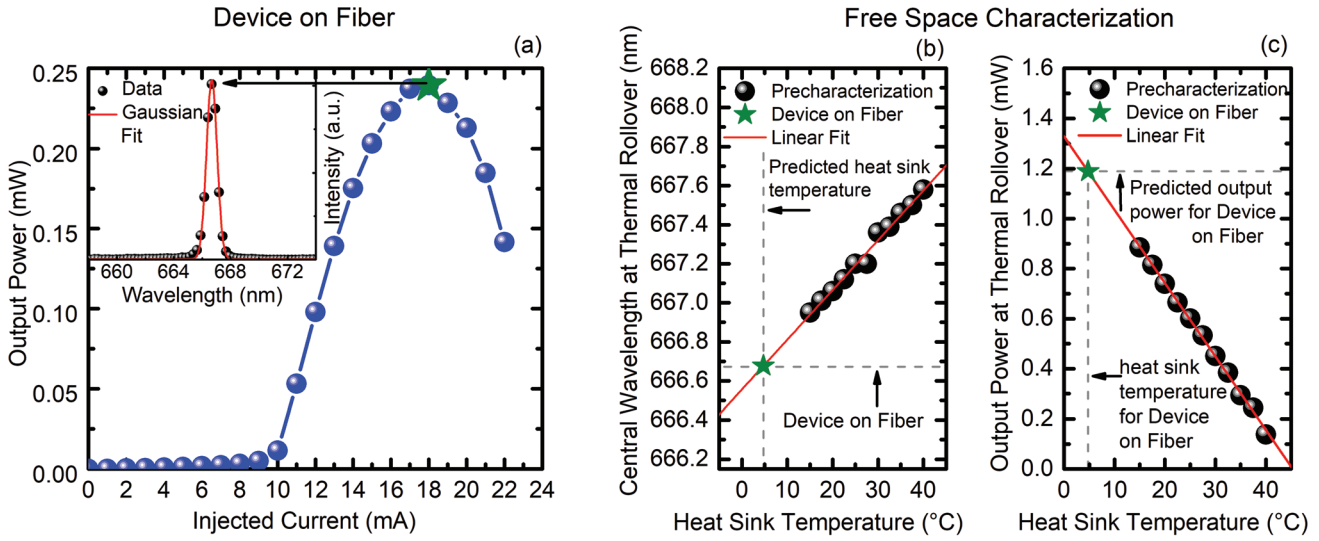


**Figure 4.** a) Output power over the injected current determining the thermal rollover for the integrated device. In the inset, the spectrum at the maximum output is exemplary shown. b) Behavior of the central emission wavelength at thermal rollover at various heat sink temperatures for the free space device (data from Figure 1c). c) Output power at thermal rollover over heat sink temperature (data from Figure 1c). In (b) and (c), the reference value from (a) is shown.

VCSEL temperature. Therefore, this method provides the most precise characterization and comparison between free space and fiber integrated device. Figure 4b reports the measured emission spectra at thermal rollover of the laser measured in free space, for different heat sink temperatures (i.e., from the measurement in Figure 1c), showing an expected linear behavior. These values can then be compared with the emission wavelength at maximum output for the fiber-integrated device (green star in Figure 4a): interestingly, the same emission spectrum could be observed for an equivalent heat sink temperature of 4.74 °C. However, in the free space case, the lowest measured operation point was 15 °C, since lower temperatures resulted in air condensation on the sample surface: nevertheless, the expected output power would be the one potentially achieved if 4.74 °C could be set on the heat sink. Once known this equivalent temperature value, it is possible to infer the expected output power at thermal rollover: Figure 4c reports the measured maximum output power as a function of the heat sink temperature, where once again an expected linear behavior is observed (values at a thermal rollover from Figure 1c). Therefore, the measured output power for the fiber-integrated device (0.24 mW) is normalized to its equivalent counterpart in the free space case (1.19 mW): this results in an in-coupling efficiency of 20.12%. The described approach compares free space to fiber integrated devices taking into account only absolute parameters that are device-temperature dependent, therefore providing the most reliable estimation of light in-coupling.

Interestingly, these measurements further show that the heat dissipation is more efficient when the VCSEL is integrated on the fiber, rather than when it is measured in free space placed over the thermal sink. This rather counterintuitive observation can be understood considering that the device performances are dependent from the local device temperature and not by the overall chip one. When integrated on the fiber, the VCSEL is surrounded by the refractive index matching medium that is more efficient in dissipating the heat rather than air (i.e., when the laser is in free space). This represents an interesting perspective for future experiments, being the performances not limited by the air thermal dissipation.

Finally, we further validated the fabrication approach by comparing the measured beam profile for the free-space and fiber-integrated case. To this aim, far-field images were measured (see Supporting Information for the setup description). All measured VCSEL showed a toroidal-shaped beam profile (**Figure 5**a), due to the laser design. Indeed, a smaller oxide aperture (see Figure 1a) would result in a Gaussian-shaped emission at the expense of the maximally achievable output power. Here, we decided to aim for the highest output having a clearly recognizable beam profile pattern. This becomes useful when comparing the free space operation with the integrated device beam profile: Figure 5b has been acquired by replacing the power meter with a beam profiling camera at the output of the multimode fiber. Although the output beam shape of a multimode fiber depends on the wave-guiding conditions of the fiber itself, a toroidal-shaped emission is still observed pointing toward the fact that a good alignment of the VCSEL over the core of the fiber has been achieved. Various tests with different multimode fibers and sources were performed (see Supporting Information). Still, a beam profile similar to the in-coupled one supports the conclusion regarding the toroidal beam profile and hints toward a good alignment in the multimode fiber core. Furthermore, a scattered pattern similar to speckle is observed due to the interference from several modes supported by the multimode fiber. We also know, however, that UV microstructuring may have a detrimental impact on the surface of the fiber tip. While this effect cannot be seen directly in the far-field after propagation, since the speckle due to mode interference is dominating, it can still impact the device performances. Interestingly, this issue can be solved in the future by replacing the laser ablation step with a lift-off process, when opening the metal in correspondence with the fiber core. This would maintain unaltered the fiber core properties. In addition, we cannot exclude that intermixing between the refractive index matching glue and the epoxy may have occurred. For this reason, future devices will be fabricated employing a high accuracy flip-chip bonder capable of disposing glues with higher precision (here done by hand). This would allow for a further improvement of the observed light coupling.

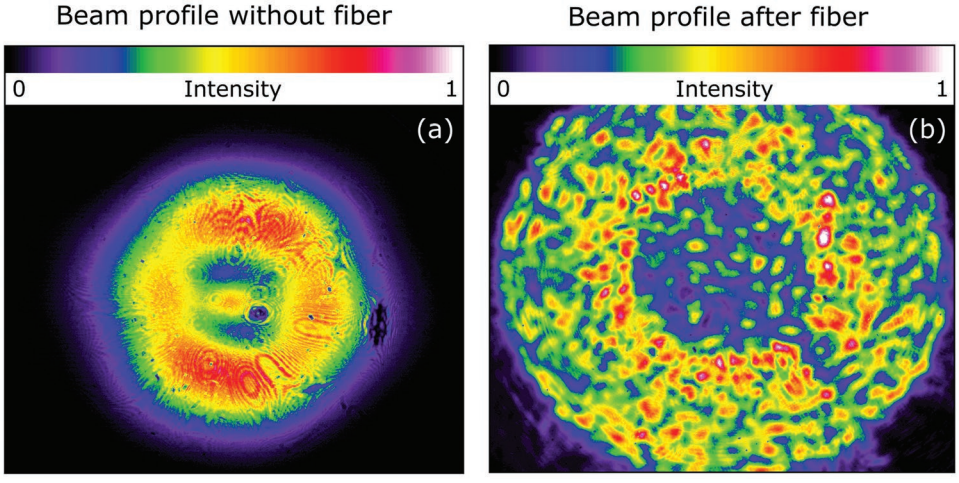


**Figure 5.** a) Beam profile of the selected VCSEL measured for the free space device. b) Beam profile of the selected VCSEL after integration on the fiber. The symmetry of the profile is similar to the free space measurement in (a) but interference is present.

## 3. Discussion and Conclusion

In this work, we demonstrated a novel method to deterministically integrate small foot-print electrically driven light sources directly on the fiber-tip. The metallization of the ferrule with subsequent laser-machining of the deposited metal, enabled the realization of alignment markers and apertures around the fiber core. A refractive index matching glue was deposited onto the fiber core to minimize insertion losses (due to refractive-index mismatch), while a conductive epoxy was deposited onto the metallized area to enable the electrical contacts. The markers allowed the deterministic alignment, with sub-micrometric precision, of the active area of the optoelectronic chip on the fibre core. To demonstrate the effectiveness of our technique and provide a proof-of-concept, a QW-VCSEL was successfully integrated onto the fiber tip, and its emission characteristics were compared before and after the fabrication process: an in-coupling efficiency of >20% was experimentally observed. Far field measurements suggested that the correct laser alignment was achieved and, interestingly, the integration procedure enables a more efficient heat dissipation, lowering the achievable laser operation temperature. These proof-of-principle experiments validate the effectiveness of the technique for integrating optoelectronic chips directly on the fiber tip. Different to pigtailed fiber diodes that are currently the main choice on market, in our configuration the light is directly coupled to the fiber without using additional optics, drastically minimizing the overall device footprint. Moreover, the device is electrically connected to the metalized fiber without using additional wire bonding, with an unprecedented degree of mechanical stability, making the optoelectronic probe suitable for use in harsh environments.

Although in this work the transferring step of the chip onto the fiber tip was carried out manually (by means of a vacuum pick-up tool and an optical microscope), our technology is fully compatible with large-scale industrial processing. For future realizations, the use of sub-micron die bonder with an automatic manipulator will allow for reliable mass production, guaranteeing at the same time, the high level of accuracy and effective attachment of chips to fibers. This approach will also allow to solve the tradeoff between complexity and accuracy in the assembly of fibers to photonic chips, which currently limits the realization of high-efficiency optical packaging and integrated systems.[30]

Moreover, Lab-on-Fiber technology offers the possibility to apply the nano-fabrication approaches directly onto the optical fiber tip, allowing for the realization of complex nanostructures for controlling the flow of light,[4] also in 3D.[5] In this specific context, Lab-on-Fiber technology could be judiciously exploited to realize optical fiber lenses,[31] improving the light coupling efficiency, and avoiding misalignment issues. Specifically, different types of miniaturized lenses (metalenses) could be designed to modify the numerical aperture (NA) of the fiber, such as: i) both metallic[32] and dielectric[33,34] nanostructures consisting of sub-wavelength elements written by lithographic techniques[35]; ii) Fresnel lenses written through direct laser writing based on two photon polymerization[36,37]; iii) microlenses embedded into the fiber tip by means of focused ion beam approach.[38,39] Moreover, Lab-on-Fiber technology could be also exploited for realizing antireflection coatings, directly onto the fiber tip, before the metal deposition.[40,41] With that method, it could be possible to avoid the use of refractive index matching glue and simplifying the overall process.

Concerning the definition of the fiber aperture and alignment markers, the use of laser micromachining, albeit interesting, may still induce roughness on the fiber surface, which can limit the achievable coupling efficiency. This can be avoided replacing the laser machining step with two photon lithography approaches which in turn are fully consistent also for the integration of 3D metalenses on the termination of optical fibers[42]. An alternative approach is based on lift-off processes assisted by electron beam lithography for opening the metal in correspondence with the fiber core. Focused Ion Beam milling can be used as well,[43,44] however the limited write field could lead to some stitching or misalignment issues during the definition of the markers, when large-area optical fibers are employed.

The use of single-mode fibers, with their smaller core diameter, would require a much higher precision in the positioning and integration of the chip. This can be achieved with commercial machines, like flip-chip bonders, which can provide a placement precision reaching 500 nm. The used QW-VCSEL has a toroidal profile but reducing the aperture would confine more the current flow, resulting in a Gaussian mode profile, at the expense of the emitted power. In any case, mode matching can be obtained using microlenses able of modifying the laser light beam profile in order to match the fiber one, and increase the coupling efficiency.[31] As mentioned before, microlenses can be fabricated onto the laser surface or onto the fiber tip by exploiting different strategies. In particular, two-photon polymerization techniques are currently carried out by using commercial equipment[36,37] demonstrating the capability to translate the lens-to-laser and lens-to-fiber integration procedures into a high throughput process, compatible with industrial applications.

As the proposed technique can be easily extended to integrate a vast range of optoelectronic devices and photonic components, our work can be considered as a fundamental building block for the development of portable, plug and play, autonomous optical fiber platforms able to sense, elaborate, and transmit sensorial data in remote locations without needing connection to any bulky instrumentation. In principle, ultra-compact processing and long-range communication unit (Wi-Fi modules) could be directly integrated to the optical fiber, ensuring reliable communications without complex wiring systems. This approach could allow to break new grounds in many strategic sectors such as Wearable Technology, IoT Systems, and Telemedicine, just to name a few. Moreover, the development of all-in-fiber active optoelectronics platforms, perfectly integrated inside a customized microfluidic environment, could allow to increase the level of compactness, avoiding all those critical components (bulky sources and detectors, lenses, fiber tapers, grating couplers) that strongly affect the performances of current lab-on-a-chip devices and consequently the development of effective point-of-care platforms.[45] Finally, our results could have an important impact even in quantum technology being the integration approach transferable to electrically driven nonclassical light sources: the use of this approach with semiconductor quantum dots could enable the implementation of the most efficient, compact, and mechanically stable source of on-demand quantum light. This would require a further

improvement of the coupling efficiency and the use of single-mode fibers. These goals are within reach if the integration is performed with high-precision machines for the transfer and bonding of the chip onto the fiber.

## 4. Experimental Section

*Fabrication of the QW-VCSEL*: The QW-VCSEL was grown by MOVPE in an Aixtron 3 × 2 inch closed coupled showerhead reactor on an n-doped gallium arsenide wafer. A bottom n-doped distributed Bragg reflector (DBR) was first realized using $Al_{0.5}GaAs/Al_{0.95}GaAs$ alternating layers with thickness chosen to maximize the reflectivity for the red spectral range. Then, an active region based on GaInP QWs in $Al_{0.33}GaInP/Al_{0.55}GaInP$ barriers was deposited. The sample was then covered with a top p-doped DBR also based on alternating $Al_{0.5}GaAs/Al_{0.95}GaAs$ layers including an $Al_{0.98}GaAs$ oxidation layer. In order to realize the employed VCSEL structure, optical lithography (Karl Suss mjb-3 mask aligner) was utilized to define circular etching masks. Wet chemical etching defined the wanted mesa structures. To define the area of current flow and optical confinement, wet thermal oxidation of the $Al_{0.98}GaAs$ layer was used. A second optical lithography step defined the geometry of the isolation layer. Final optical lithography, metal deposition, and lift-off steps defined the top p-contact geometry while the bottom substrate was metallized to form the n-contact. The electrically driven VCSEL sample was cleaved into pieces of roughly 500 μm × 500 μm. After the cleaving step, the samples were cleaned in acetone and isopropanol to remove contaminants from the surface. All samples possessed four lasers with a 170 μm × 170 μm metal area on the p-side, which will go in contact with the gold coating of the fiber after the gluing process.

## Supporting Information

Supporting Information is available from the Wiley Online Library or from the author.

## Acknowledgements

The authors acknowledge Stephan Schmiel for the support in the device fabrication.

Open access funding enabled and organized by Projekt DEAL.

## Conflict of Interest

The authors declare no conflict of interest.

## Author Contributions

A.R. and M.Z. contributed equally to this work. A.M., F.P., and M.G. prepared the utilized fiber with the support of A.R. and A.C. M.Z., N.W., and M.K. realized the integration of the sample grown by M.J. M.Z. and N.W. performed the experiment with the support of S.L.P. A.R. and S.L.P. designed the experiment with the support of A.C. and P.M. A.R., A.C., P.M., and S.L.P. supervised the project. The manuscript was written through contributions of all authors. All authors have given approval to the final version of the manuscript.

## Data Availability Statement

The data that support the findings of this study are available from the corresponding author upon reasonable request.

## Keywords

lab-on-fiber technology, optical fibers, optoelectronic devices, quantum-well vertical-cavity surface-emitting laser

Received: December 30, 2021
Revised: February 24, 2022
Published online: March 18, 2022

[1] B. Temelkuran, S. D. Hart, G. Benoit, J. D. Joannopoulos, Y. Fink, *Nature* **2002**, *420*, 650.
[2] P. Russell, *Science* **2003**, *299*, 358.
[3] A. F. Abouraddy, M. Bayindir, G. Benoit, S. D. Hart, K. Kuriki, N. Orf, O. Shapira, F. Sorin, B. Temelkuran, Y. Fink, *Nat. Mater.* **2007**, *6*, 336.
[4] A. Cusano, M. Consales, A. Crescitelli, A. Ricciardi, *Lab-on-Fiber Technology*, 1st ed., Springer International Publishing, Switzerland **2015**, p. 359.
[5] J.-Y. Rauch, O. Lehmann, P. Rougeot, J. Abadie, J. Agnus, *J. Vac. Sci. Technol., A* **2018**, *36*, 041601.
[6] T. Gissibl, S. Thiele, A. Herkommer, H. Giessen, *Nat. Photonics* **2016**, *10*, 554.
[7] P. Vaiano, B. Carotenuto, M. Pisco, A. Ricciardi, G. Quero, M. Consales, A. Crescitelli, E. Esposito, A. Cusano, *Laser Photonics Rev.* **2016**, *10*, 922.
[8] H. Pahlevaninezhad, M. Khorasaninejad, Y.-W. Huang, Z. Shi, L. P. Hariri, D. C. Adams, V. Ding, A. Zhu, C.-W. Qiu, C. Federico, M. J. Suter, *Nat. Photonics* **2018**, *12*, 540.
[9] J. A. Guggenheim, J. Li, T. J. Allen, R. J. Colchester, S. Noimark, O. Ogunlade, I. P. Parkin, I. Papakonstantinou, A. E. Desjardins, E. Z. Zhang, P. C. Beard, *Nat. Photonics* **2017**, *11*, 714.
[10] A. Aliberti, A. Ricciardi, M. Giaquinto, A. Micco, E. Bobeico, V. L.a Ferrara, M. Ruvo, A. Cutolo, A. Cusano, *Sci. Rep.* **2017**, *7*, 14459.
[11] M. Giaquinto, A. Aliberti, A. Micco, F. Gambino, M. Ruvo, A. Ricciardi, A. Cusano, *ACS Photonics* **2019**, *6*, 3271.
[12] M. Pisco, F. Galeotti, G. Quero, G. Grisci, A. Micco, L. V. Mercaldo, P. Delli Veneri, A. Cutolo, A. Cusano, *Light: Sci. Appl.* **2017**, *6*, e16229.
[13] M. Principe, M. Consales, A. Micco, A. Crescitelli, G. Castaldi, E. Esposito, V. L.a Ferrara, A. Cutolo, V. Galdi, A. Cusano, *Light: Sci. Appl.* **2017**, *2017*, e16226.
[14] A. Xomalis, I. Demirtzioglou, E. Plum, Y. Jung, V. Nalla, C. Lacava, K. F. MacDonald, P. Petropoulos, D. J. Richardson, N. I. Zheludev, *Nat. Commun.* **2018**, *9*, 182.
[15] P.-I. Dietrich, M. Blaicher, I. Reuter, M. Billah, T. Hoose, A. Hofmann, C. Caer, R. Dangel, B. Offrein, U. Troppenz, M. Moehrle, W. Freude, C. Koos, *Nat. Photonics* **2018**, *12*, 241.
[16] H. Gehring, M. Blaicher, W. Hartmann, P. Varytis, K. Busch, M. Wegener, W. H. P. Pernice, *APL Photonics* **2019**, *4*, 010801.
[17] R. He, P. J. A. Sazio, A. C. Peacock, N. Healy, J. R. Sparks, M. G. V. Krishnamurthi, J. V. Badding, *Nat. Photonics* **2012**, *6*, 174.
[18] M. Rein, V. Favrod, C. Hou, T. Khudiyev, A. Stolyarov, J. Cox, C.-C. Chung, C. Chhav, M. Ellis, J. Joannopoulos, Y. Fink, *Nature* **2018**, *560*, 214.
[19] Y.-F. Xiong, J.-H. Chen, Y.-Q. Lu, F. Xu, *Adv. Electron. Mater.* **2019**, *5*, 1800562.
[20] Y. F. Xiong, Q. B. Liao, Z. P. Huang, X. Huang, C. Ke, H. T. Zhu, C. Y. Dong, H. S. Wang, K. Xi, P. Zhan, F. Xu, Y. Q. Lu, *Adv. Mater.* **2020**, *32*, 1907242.
[21] J. P. Seurin, in *VCSELs: Fundamentals, Technology and Applications of Vertical-Cavity Surface-Emitting Lasers*, (Ed: R. Michalzik), Vol. *166*, Springer Series in Optical Sciences, Springer, Berlin, Heidelberg **2013**.

[22] M. Grabher, R. Jäger, R. Michalzik, B. Weigl, G. Reiner, K. Ebeling, *IEEE Photonics Technol. Lett.* **1997**, *9*, 1304.
[23] T. Sarmiento, L. Zhao, P. Moser, T. Li, Y. Huo, J. Harris, *IEEE Photonics Technol. Lett.* **2019**, *31*, 1607.
[24] R. Stevens, A. Risberg, R. Schatz, R. M. von Wuertemberg, B. Kronlund, M. Ghisoni, K. P. Streubel, in *Proc. SPIE 3946, Vertical-Cavity Surface-Emitting Lasers IV*, International Society for Optics and Photonics, San Jose **2000**.
[25] N. Gisin, G. Ribordy, W. Tittel, H. Zbinden, *Rev. Mod. Phys.* **2002**, *74*, 145.
[26] C. Degen, F. Reinhard, P. Cappellaro, *Rev. Mod. Phys.* **2017**, *89*, 035002.
[27] T. H. Chung, G. Juska, S. T. Moroni, A. Pescaglini, A. Gocalinska, E. Pelucchi, *Nat. Photonics* **2016**, *10*, 782.
[28] M. Sartison, S. Seyfferle, S. Kolatschek, S. Hepp, M. Jetter, P. Michler, S. L. Portalupi, *Appl. Phys. Lett.* **2019**, *114*, 222101.
[29] T. Müller, J. Skiba-Szymanska, A. B. Krysa, J. Huwer, M. Felle, M. Anderson, R. M. Stevenson, J. Heffernan, D. A. Ritchie, A. J. Shields, *Nat. Commun.* **2018**, *9*, 862.
[30] P. Cheben, R. Halir, J. H. Schmid, H. A. Atwater, D. R. Smith, *Nature* **2018**, *560*, 565.
[31] F. Piccirillo, M. Giaquinto, A. Ricciardi, A. Cusano, *Results in Optics* **2022**, *6*, 100203.
[32] M. Khorasaniejad, F. Capasso, *Science* **2017**, *358*, no. p. eaam8100.
[33] O. Yermakov, H. Schneidewind, U. Hübner, T. Wieduwilt, M. Zeisberger, A. Bogdanov, Y. Kivshar, M. A. Schmidt, *ACS Photonics* **2020**, *7*, 2834.
[34] C. Zhou, W.-B. Lee, S. Gao, H. Li, C.-S. Park, D.-Y. Choi, S.-S. Lee, *Laser Photonics Rev.* **2021**, *15*, 2170028.
[35] P. Genevet, F. Capasso, F. Aieta, M. Khorasaninejad, R. Devlin, *Optica* **2017**, *4*, 139.
[36] M. Plidschun, H. Ren, J. Kim, R. Förster, S. A. Maier, M.. Schmidt, *Light: Sci. Appl.* **2021**, *10*, 57.
[37] A. Asadollahbaik, S. Thiele, K. Weber, A. Kumar, J. Drozella, F. Sterl, A. M. Herkommer, H. Giessen, J. Fick, *ACS Photonics* **2019**, *7*, 88.
[38] H. Melkonyan, K. Sloyan, M. Odeh, I. Almansouri, M. Chiesa, M. S. Dahlem, *J. Phys.: Photonics* **2019**, *1*, 025004.
[39] H. Melkonyan, K. Al Qubais, K. Sloyan, A. Khilo, M. S. Dahelm, *Opt. Express* **2017**, *25*, 13035.
[40] P. Spinelli, M. Verschuuren, A. Polmann, *Nat. Commun.* **2012**, *3*, 692.
[41] M. Scaravilli, A. Micco, G. Castaldi, G. Coppola, M. Gioffrè, M. Iodice, V. L.a Ferrara, V. Galdi, A. Cusano, *Adv. Opt. Mater.* **2018**, *6*, 1800477.
[42] W. Hadibrata, H. K. S. Wei, K. Aydin, *Nano Lett.* **2021**, *21*, 2422.
[43] A. Micco, A. Ricciardi, M. Pisco, V. L.a Ferrara, A. Cusano, *Sci. Rep.* **2015**, *5*, 15935.
[44] M. Consales, G. Quero, S. Spaziani, M. Principe, A. Micco, V. Galdi, A. Cutolo, A. Cusano, *Laser Photonics Rev.* **2020**, *14*, 2000180.
[45] H. Yang, M. A. Gijs, *Chem. Soc. Rev.* **2018**, *47*, 1391.